Defect Printability and Inspectability of Halftone Masks for the 90nm and 70nm Node

Karin Eggers[a], Karsten Gutjahr[a], Milko Peikert[a], Dieter Rutzinger[a], Ralf Ludwig[b], Michael Kaiser[b], Jan Heumann[b]
[a] Infineon Technologies AG, Königsbrücker Str. 180, 01099 Dresden, Germany
[b]Advanced Mask Technology Center, Rähnitzer Allee 9, 01109 Dresden, Germany

Abstract

In this paper we will present first results of a defect printability study undertaken for the 70nm technology. Therefor 6% halftone, programmed defect test mask, that contain dense l/s structures were exposed at different production illumination conditions and the outcoming data were compared to the related defect sizes on mask, AIMS and inspection data. As expected over and under sizing of features are the most print and AIMS critical structures. Dark and clear extensions show on wafer as on AIMS very similar behavior.
Additionally to the determination of the print critical AIMS values the defect masks were used for the evaluation of a new defect inspection system. The performance of two detection pixels P125 and P90 as also of two inspection modes d2dT and d2dR was investigated on 90nm and 70nm dense l/s and CH areas respective to the print results. Over and under sizing of small dense structures as also dark and clear defects centered in a clear or dark structure are challenging for the new inspection tool. D2dR mode shows a better performance for dense contact hole arrays than d2dT.

Keywords: mask, defect, printability, AIMS, inspection system

1 Introduction

193nm optical lithography is being extended to the 70nm node and beyond. To realize feature sizes less than half of the exposure wavelength, halftone masks with a variety of illumination settings are being utilized. As defect printability is very much dependent on the exposure conditions defect printability studies are essential for the production of lithographically “defect-free” masks. The pattern inspection needs to ensure that all critical defects are found. Nowadays aerial imaging microscopy is widely used inside the mask shops for dispositioning of defects according to defect printability criteria.
In this study wafer data of a 70nm dense l/s defect array with programmed defects were collected and analized. We used for the 70nm array two different illumination settings. The assessment if a defect prints or not was done by wafer CD SEM measurements and review of the taken SEM pictures. For print critical defects the mask defect sizes were calculated. For collecting the AIMS data the same sigma settings were used as for print studies.
Through the correlation of the three parameters, wafer CD, AIMS value and defect size a so-called AIMS criteria for print critical defects can be defined.
Since print critical defects have not only to be characterized but also to be detected we describe here first sensitivity results for a new mask inspection tool. For programmed defects in 90nm and 70nm dense l/s and contact arrays a sensitivity analysis was compared to the wafer prints. The inspection tool evaluation was done for two different detection pixel sizes and two modes.

2 Experimental

The work presented in this paper is based upon two different MoSi-quartz patterns (see Fig. 1 and 2) containing different types of defects, for each of which different defect sizes were programmed. The design of Fig. 1 is two times realized on the mask, for 70nm and 90nm dense l/s. A second pattern die without programmed defects was placed onto the mask in order to perform die-to-die inspections.

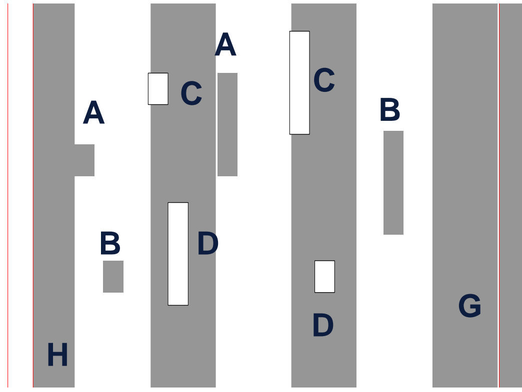

Fig. 1 Layout for dense 90nm and 70nm l/s array with programmed defects. Defect types: A: dark extension (DEX), B: dark center (DCE), C: clear extension (CEX), D: clear center (CCE), G: over sizing (OVER), H: under sizing (UNDER).

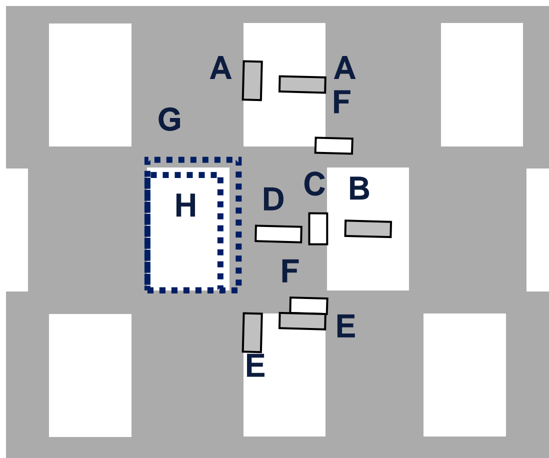

Fig. 2 Layout for dense 70nm contact hole array with programmed defects. Defect types: A: dark extension (DEX), B: dark center (DCE), C: clear extension (CEX), D: clear center (CCE), E: dark corner (DCO), F: clear corner (CCO), G: over sizing (OVER), H: under sizing (UNDER).

Both patterns (Fig.1 and Fig. 2) were printed using the optimized scanner conditions to reach the best results on wafer. The 70nm dense l/s area was exposed under disar and quasar sigma settings. CD changes caused by the corresponding defects were measured out at a wafer CD SEM. Additionally the SEM images were reviewed.

For the 70nm dense l/s array the mask defect sizes were determined by using the "square root area" (SRA) method. SRA method measures the square root of an estimated defect area.

AIMS measurements were performed by using the exposure tool or very similar conditions. AIMS values were measured using the intensity profile for a line orientated perpendicular to the pattern line where the defect was located. The intensity profiles were optimized to achieve a maximum intensity deviation between the defective and defect-free areas. AIMS values were determined by measuring the peak intensities of the defective and defect-free area and calculating the percentile intensity deviation of both intensities.

The 90 and 70nm dense l/s layouts and the 70nm dense CH area on the programmed defect test masks (Fig.1 and 2) were used to investigate the mask inspection tool KLA TeraScan 52x. "Die-to-die" transmittive (d2dT) and reflective (d2dR) algorithm in combination each with the detection pixels 90nm and 125nm were evaluated referring to the print results. At die-to-die inspections defects were localized by comparison of a defected die with a defect-free die.
The defect sensitivity of the algorithms was determined by inspecting the programmed defect area of a certain test mask ten times. Sensitivity analysis was performed using the exact coordinates of a programmed defect. A matching rage of 10µm was used to ensure that only the programmed defects were considered.

3 Results

3.1 Print Results vs. AIMS Values and Defect Sizes

A printability study of a dense 70nm l/s array for quasar and disar exposure conditions was performed. Mask SEM and AIMS images of the defects were analyzed and correlated to the printed wafer CD SEM data and images.
Presented defect results are related to dark and clear extensions and over respectively under sizing of main dense line features. The extensions are the most common on mask and over and under sizing have the biggest impact on wafer.
The relation between the AIMS value and the defect size is given for the extensions in Fig. 3 and 4. The two charts present the AIMS values for defected structures by using a quasar sigma setting. Very similar results were received for disar sigma stopper settings. The slope of the linear fit in chart 4 is slightly steeper as that in Fig. 3. But the observed printing behavior of dark and clear extensions is the same. Actual AIMS values for the smallest printing defects of these two defect types are similar.
The observed correlation between AIMS value and defect size is not very precise. Reason is that the measuring failure for the defect size as also the AIMS

intensity deviations lying in the range of the absolute value.

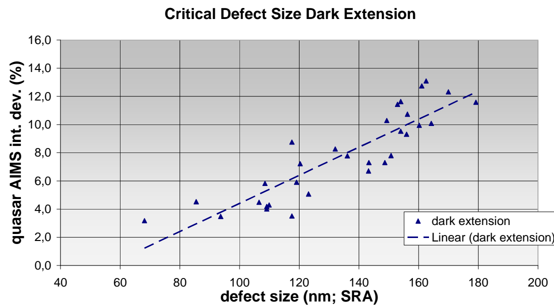

Fig. 3 AIMS values for dark extension defects received with quasar sigma settings were plotted with respect to defect sizes measured by the SRA method. The chart contain data of "quadratic" and "rectangular" (long) designed dark extensions.

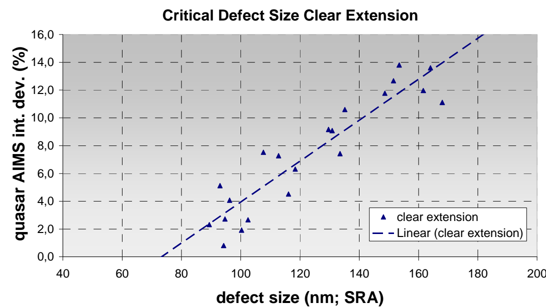

Fig. 4 AIMS values for clear extension defects received with quasar sigma settings were plotted with respect to defect sizes measured by the SRA method. The chart contained data of "quadratic" and "rectangular" (long) designed clear extensions.

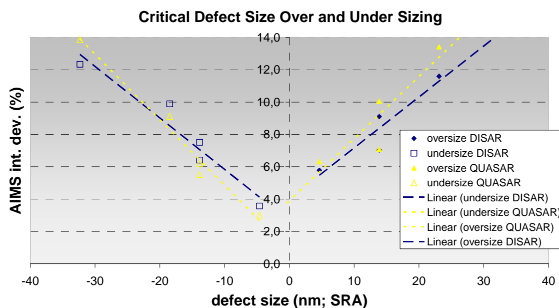

Fig. 5 AIMS values for over and under sizing of dense line features were plotted with respect to defect sizes measured by the SRA method. AIMS data for quasar and disar settings were compared.

Over and under sizing of main features, in our case dense lines/spaces, are the most print critical structures. Fig. 5 presents the AIMS intensity deviation of these defect types versus the defect size for quasar and disar AIMS settings. The slope of the linear fit is for quasar settings slightly stronger as for disar. This means the AIMS value of a print critical defect with a certain size is for quasar stopper higher than for disar conditions. Different "print critical" AIMS criteria have to be defined for disar and quasar settings. Slopes for fits within the same AIMS exposure setting are very identical.

Since the AIMS/wafer CD correlation was very poor the wafer SEM images of the defects were reviewed and compared to the corresponding AIMS intensity. Non-printing defects were allocated to the figure "0". Printing defects got the digit "1". In Fig. 6 and 7 the disar AIMS intensity deviation is plotted against the defect printability severity "0" and "1". The print critical AIMS value for both extension types is situated between 9% and 10%. Similar results were received for the quasar conditions.
Over and under sizing defects impact the wafer result much more than all other defect types (Fig. 8). Under quasar conditions the lowest print critical AIMS value was received with ~5,5% for under sizing. In general quasar conditions show lower print critical AIMS values than disar options and under sizing is more severe than over sizing.

3.2 Defect Sensitivity Regarding Printability Results

In this part the performance of the KLA inspection tool TeraScan 52x was compared to printing results. The inspection modes die-to-die reflective (d2dR) and transmittive (d2dT) each combined with detection pixel 125nm (P125) and 90nm (P90) were tested on dense 70nm and 90nm node l/s features (Fig. 1) and a 70nm contact hole array (Fig.2).
The inspection tool sensitivity settings for d2dT and d2dR with P125 were kept at 100%. For P90 sensitivity settings very near 100% were chosen such that the number of false and nuisance defects was reasonable.

Fig. 9, 10 and 11 present the results of the four inspection combinations (d2dT P125, d2dR P125, d2dT P90 and d2dR P90) and the print results of the two dense l/s areas and the contact array referring to different defect types (Fig. 1, Fig. 2). The smallest "design" defect size detected with 100% capture rate and the smallest "design" printing defect were plotted against different defect types. "Design" defect size is the size of which a defect was layouted and does not correspond the actual size. On the x axis kinds of defect types with their short cut name are shown (see Fig. 1 and 2). The red curve present the printing base line for each defect type. The four inspection mode combinations are expressed by 4 different marks.

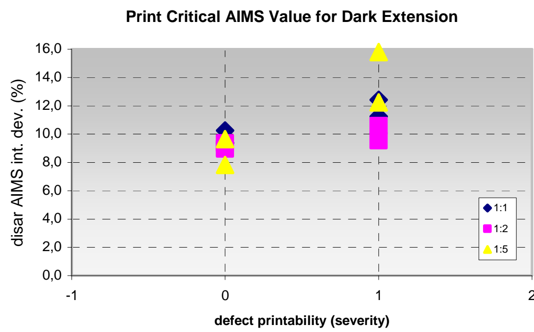

Fig. 6 Dark extensions: AIMS values for print critical ("1") and non-critical ("0") defects at disar exposure and AIMS settings; designed width to length relation of defects is 1:1 or 1:2 or 1:5.

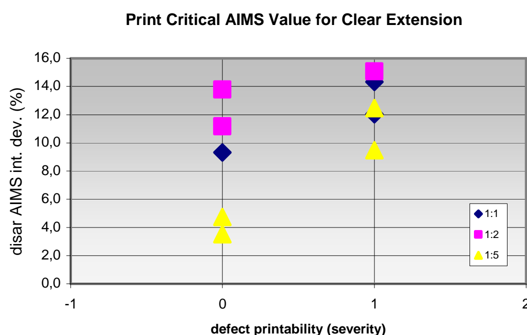

Fig. 7 Clear extensions: AIMS values for print critical ("1") and non-critical ("0") defects at disar exposure and AIMS settings; designed width to length relation of defects is 1:1 or 1:2 or 1:5.

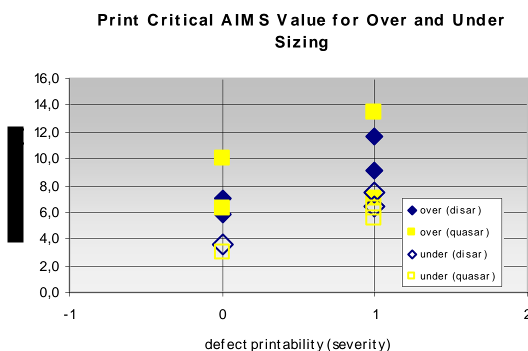

Fig. 8 Over and under sizing: AIMS values for print critical ("1") and non-critical ("0") defects at disar and quasar exposure and AIMS settings.

A certain defect type was not sufficient detected if the red defect print line is plotted at an lower level than the mark of the used inspection combination. Are the print line and the detection mark on the same level the defect capturing is still critical, since for productive masks sensitivity settings have often to be lowered and so the full capture rate of the smallest detected and printed defect is not given any more.

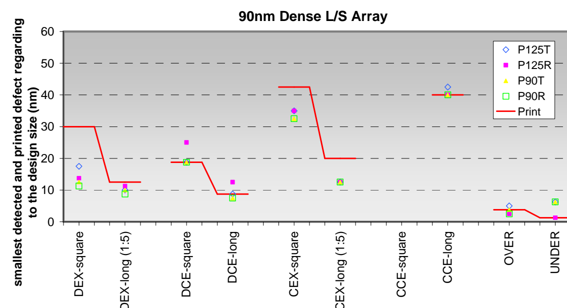

Fig. 9 Sensitivity analysis for 90nm dense l/s array: Smallest printing and smallest detected defect captured by 100% for four inspection modes (P125 d2dT, P125 d2dR, P90 d2dT and P90 d2dR) is plotted against different types of defects (Fig 1).

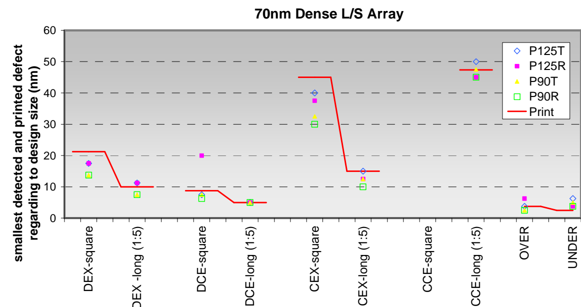

Fig. 10 Sensitivity analysis for 70nm dense l/s array: Smallest printing and smallest detected defect captured by 100% for four inspection modes (P125 d2dT, P125 d2dR, P90 d2dT and P90 d2dR) is plotted against different types of defects (Fig. 1).

Regarding the 90nm and 70nm dense l/s array none of the four inspection mode combinations captures all print critical defects. The new inspection tool has less sensitivity towards dark (DCE) and clear center (CCE) defects. A blindness for any size of squaric designed clear center defects could be detected on both dense l/s cases.

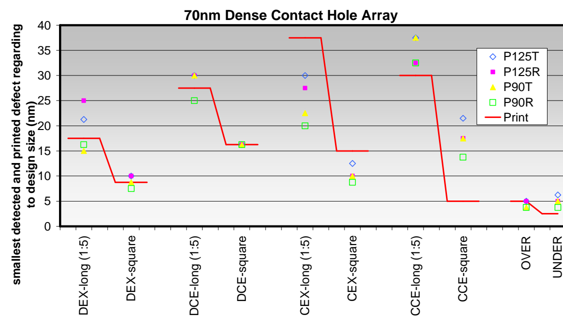

Fig. 11 Sensitivity analysis for 70nm dense contact hole array (Fig. 2): Smallest printing and smallest detected defect captured by 100% for four inspection modes (P125 d2dT, P125 d2dR, P90 d2dT and P90 d2dR) is plotted against different types of defects.

In contrary to center defects that are relative rare on masks, over and under sizing of structures, is frequently and presents the most critical impact on wafer (refer to Fig. 8 and 5). All four inspection variations show a capture risk for over sizing and a leak for under sized structures.

The reflective modes show a slight advantage against the transmittive mode reagarding the under sizing detection.

In general the sensitivity within dense l/s structures for so-called long defects, which have a width to length size relation of 1:5 is less than for squaric ones. This effect is inverted at the investigated dense contact areas.

Overall sensitivity of the tool for different printing defects in a dense array of small contact holes is poorer than for dense l/s features (Fig.11, 10 and 9).

For all investigated defect types except the well catched clear extensions a risk of no capture is existing at the used sensitivity settings or at applying slightly desensed adjustments. For clear center defects and over respectively under sized structures it could spoken of a capture leak.

4 Summary

Using systematic programmed defect arrays the true impact of defect types and sizes on the wafer can be measured and compared to the detection and assessment methods used within the mask shops and wafer fabs.

The printing results of a programmed 70nm dense l/s array were compared with the AIMS data and defect sizes on masks. The determined correlation between the three parameters, AIMS value, defect size and CD change on wafer was poorer than for former technology nodes. Reason was that the intensity deviations of the AIMS tool, the inaccuracy at the determination of the defect size on mask, the mask CD uniformity deviations and the litho process variations have in worst case the same range than the defect impact. For future more statistical measurements are necessary.

The differences of clear and dark extensions in their behaviour on wafer and AIMS intensity were negligible. Also the influence of the sigma conditions of the exposures on wafer prints was less but a change of the sigma settings for an AIMS tool can drastically switch AIMS intensity values.

The most critical defects with impact on wafer are as expected the over and under sizing of structures. Here we saw the smallest print critical AIMS intensity values.

For sensitivity testing of the KLA TeraScan 52x the print results of three array features (70nm and 90nm dense l/s and 70nm dense contact hole arrays) were compared with the defect detection capability of the tool by using four inspection mode settings (d2dR P125, d2dT P125, d2dR P90 and d2dR P90).

None of the four tested inspection mode combinations can deal with the whole printing variety of programmed defects on all three arrays. As expected P90 shows better sensitivity compared to P125.

D2dR shows improved sensitivity for the 70nm dense CH array defects whereas the benefit for the l/s layers is not very strong formed except for better capturing of undersized structues.

The sensitivity leak of the tool towards over sizing and especially under sizing of structures for the investigated array types is very critical. Also the capture rate for defects within the contact array is lower than for the dense l/s features.

5 Acknowledgements

Thanks has to be brought to Annett Helm, from IFX Dresden and Melanie Lewik, from IFX Dresden for mask layout and Martin Verbeek, from IFX Munich for AIMS discussions.